Hindawi Publishing Corporation
International Journal of Photoenergy
Volume 2015, Article ID 708048, 7 pages
http://dx.doi.org/10.1155/2015/708048

Research Article

Structural Dependence of Electronic Properties in A-A-D-A-A-Type Organic Solar Cell Material

Ram S. Bhatta and Mesfin Tsige

Department of Polymer Science, The University of Akron, Akron, OH 44325, USA

Correspondence should be addressed to Ram S. Bhatta; rsb20@zips.uakron.edu and Mesfin Tsige; mtsige@uakron.edu

Received 27 October 2014; Accepted 12 January 2015

Academic Editor: David Worrall

Small conjugated molecules (SCMs) are promising candidates for organic photovoltaic (OPV) devices because of their structural simplicity, well control over synthetic reproducibility, and low purification cost. However, industrial development of SCM-based OPV devices requires improving their performance, which in turn relies on the fundamental understanding of structural dependence of electronic properties of SCMs. Herein, we report the structural and electronic properties of the BCNDTS molecule as a model system for acceptor-acceptor-donor-acceptor-acceptor (A-A-D-A-A) type SCMs, using density functional theory (DFT) and time-dependent DFT methods. Systematic calculations of two-dimensional potential energy surfaces, molecular electrostatic potential surfaces, ground state frontier molecular orbital energies, and the vertical excitation energies are performed. We found that the lowest energy conformation of the BCNDTS molecule is planar. The planar conformation favors the lowest ground state and the excited state energies as well as the strongest oscillator strength. The present results suggest that SCMs containing central dithienosilole cores connected with 2,1,3-benzothiadiazole groups have potential to be an efficient electron donor for OPV devices.

1. Introduction

Organic photovoltaic (OPV) devices have gained wide interest in recent years because of the world's growing demand for clean, renewable, and sustainable energy [1–3]. The promise of OPV devices derives not only from their light weight, flexibility, and environmental friendliness, but also from an expected drastic reduction of the cost associated with the electricity generation [4]. OPV devices contain two active materials: electron acceptors and electron donors. Fullerene derivatives are commonly used as electron acceptors. Electron donors are either conjugated polymers (CPs) or small conjugated molecules (SCMs). Although the current PCE of single-junction CP-based OPV devices has reached ~9% [5], CPs are suffering from various problems such as lack of synthetic reproducibility, high purification cost, and residual terminal groups of polymers [6]. A potential option to overcome these problems is the replacement of CPs by soluble SCMs [7]. Therefore, research on SCM-based OPV devices has grown very rapidly reaching the current PCE of ~7%, which is comparable to the PCE of the best CP-based OPV devices [8]. However, the PCE of SCM-based OPV devices needs to be further increased for the industrial development of OPV devices.

Various experimental studies [8–14] have been concentrated on the synthesis of SCMs and their OPV performances in recent years. Among SCMs, molecules containing central dithienosilole cores connected with 2,1,3-benzothiadiazole groups have been reported as the promising electron donors for OPV devices [8, 9]. In SCMs, typical charge carriers are holes and electrons in p-orbitals [15]. Electron transfer from SCMs to fullerene derivatives depends on the energy difference between the highest occupied molecular orbital (HOMO) and the lowest unoccupied molecular orbital (LUMO). Furthermore, HOMO and LUMO energies are affected by the accessible molecular conformations. Although the synthesis and the performance of dithienosilole-based molecule (Figure 1) are studied experimentally, the fundamental factor such as the conformational dependence of electronic properties that affect the performance of these

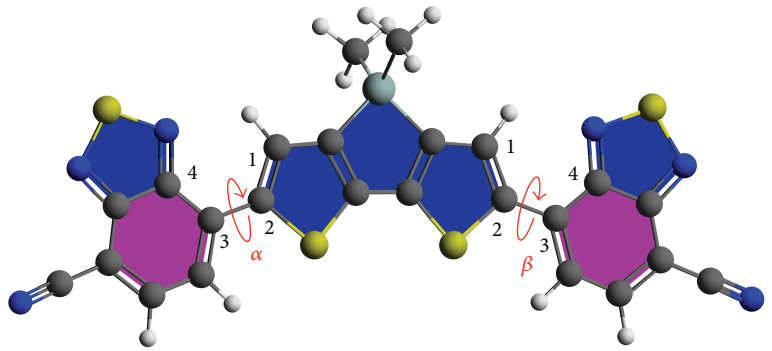

Figure 1: Structure of the BCNDTS molecule. The interring torsional angles, α and β, are zero when C–C–C–C (numbered by 1, 2, 3, and 4) angles are in cis conformations shown. In the present computations, the methyl group replaces octyl chain.

molecules remained unexplored. Thus, a necessary step of understanding the performance of SCMs in OPV application is to investigate the relative variation of conformational energies caused by the torsional defects, HOMO-LUMO gaps, and the vertical excitation energies.

In the present study, we perform first-principles calculations to investigate the structural and electronic properties of BCNDTS molecule. This work is organized as follows. Section 2 contains computational methods employed in this study. The results and discussion are presented in Section 3. Two-dimensional potential energy surface for the BCNDTS molecule is discussed in Section 3.1. Then, in Sections 3.2 and 3.3, we present surfaces of molecular electrostatic potential and HOMO-LUMO gap surfaces, respectively. Section 3.4 presents the vertical excitation energies, followed by the main conclusions of the present work in Section 4.

2. Computational Methods

The molecular structure of BCNDTS molecule studied is shown in Figure 1. The two torsional angles (α and β) are defined in terms of the relevant interring C–C–C–C dihedral angles in such a way that $\alpha = \beta = 0^\circ$ represents the molecular conformation as shown in Figure 1. Two types of geometry minimizations were performed. The first is the fully relaxed geometry optimization of BCNDTS molecule without any constraint. The second is sets of geometry optimizations at constrained values of α and β in the range of $0^\circ \leq \alpha \geq 180^\circ$ and $0^\circ \leq \beta \geq 180^\circ$. All geometry optimizations were performed using density functional theory (DFT) [16] combined with Becke's three-parameter Lee-Yang-Parr exchange-correlations functional (B3LYP) [17] as implemented in the Gaussian 09 program package [18]. The dispersion correction was implemented using Grimme approach [19]. The 6-31G(d) basis set was used with diffuse functions on all heavy atoms. The dispersion-corrected B3LYP functional was chosen because our previous study [20] on CPs has shown that it yields accurate geometry and torsional potentials. The robustness of B3LYP functional to produce accurate geometries and energies of SCMs and CPs has also been validated in similar studies [21–25].

The HOMO-LUMO gap in the ground state was computed as the energy difference between HOMO and LUMO. The vertical excitation energy from the ground state to the first singlet-excited state was computed using time-dependent density functional theory (TDDFT) [26] method starting from the ground state optimized geometry.

In the context of the present work, some computations of electronic properties were also performed using the coulomb attenuated functional (CAM-B3LYP) [27] and long-rage corrected functionals (LC-BLYP [28] and wB97XD [29]) for the sake of comparison. Table 1 summarizes the computed band gaps at different functionals for fully relaxed BCNDTS molecule. Available experimental values are also included for comparison. Different functionals give different HOMO, LUMO, and vertical excitation energies. The dispersion-corrected B3LYP provides overall good agreement with the experimental values, whereas coulomb attenuated and long-range separated functionals overestimate the values. Therefore, all the results discussed hereafter are computed at the dispersion-corrected B3LYP level unless otherwise indicated.

3. Results and Discussion

3.1. Two-Dimensional Potential Energy Surface. In the pristine BCNDTS bulk, chains conformations are controlled by intermolecular packing interactions that favor planar backbone structures. However, in the practical OPV devices, BCNDTS is heterogeneously mixed with fullerene derivatives. It is interesting to explore if there is a propensity of backbone conformational disorder in such environment. Different conformations are connected by the interring torsional motion of the backbone. Hence, computation of potential energy surface as functions of the backbone torsional angles (α and β) allow us to probe the propensities of nonplanar conformations that have relatively close in energy, kT at room temperature.

To obtain the potential energy surface, forty-nine grid points were computed at constrained values of α and β in the ranges $0 \leq \alpha \leq 180^\circ$ and $0 \leq \beta \leq 180^\circ$. Computed energies are summarized in Table 2.

Table 1: Computed energies of frontier orbitals and the band gaps at different functionals for fully relaxed BCNDTS molecule. Energies are in eV.

Methods	HOMO	LUMO	Gap (HOMO-LUMO)	Gap (optical)
CAM-B3LYP	−6.77	−2.44	4.32	2.47
LC-BLYP	−7.93	−1.59	6.34	2.79
wB97XD	−7.35	−1.94	5.41	2.55
B3LYP-D	−5.66	−3.41	2.24	2.04
Exp. [9]	−5.40	—	—	2.17

Table 2: Computed energies of BCNDTS molecule in meV at constrained values of α and β.

α/β	0	30	60	90	120	150	180
0	0.00	22.49	168.53	299.45	175.29	48.11	20.81
30	22.49	44.66	190.59	322.43	197.87	70.65	43.80
60	168.53	190.59	336.63	470.07	344.77	217.48	191.13
90	299.45	322.43	470.07	605.67	478.14	350.73	324.12
120	175.29	197.87	344.77	478.14	352.83	226.51	199.81
150	48.11	70.65	217.48	350.73	226.51	99.72	72.60
180	20.81	43.80	191.13	324.12	199.81	72.60	45.36

Then, the computed energies were fitted using (1) with one-dimensional and coupling terms:

$$V = V_0 + \sum_{n=1}^{6} k_n^{\alpha} \cos n\alpha + \sum_{n=1}^{6} k_n^{\beta} \cos n\beta + \sum_{n=1}^{2} k_n^{\alpha\beta} \cos n\alpha \cos n\beta. \quad (1)$$

In (1), V_0 is the constant and the root-mean-square residual of the final fit was 0.6 meV. The contribution of coupling terms in the fit is negligible indicating that the nearest-neighbor torsional coupling in BCNDTS molecule is negligible. Figure 2 shows the two-dimensional potential energy surface of the BCNDTS molecule as a function of the two angles α and β. The contour plot of the same data is provided in the supporting information (see Figure S1 in Supplementary Material available online at http://dx.doi.org/10.1155/2015/708048) for the sake of better visualization.

The two-dimensional potential energy surface (Figure 2) has a minimum at $\alpha = \beta = 0^{\circ}$. The surface has three local minima at $\alpha = 0^{\circ}$ and $\beta = 180^{\circ}$, $\alpha = 180^{\circ}$ and $\beta = 0^{\circ}$, and $\alpha = 180^{\circ}$ and $\beta = 180^{\circ}$, respectively. At $\alpha = \beta = 90^{\circ}$, the surface has a maximum. The maximum is connected with other four local maxima at $\alpha = 0^{\circ}$ and $\beta = 90^{\circ}$, $\alpha = 90^{\circ}$ and $\beta = 0^{\circ}$, $\alpha = 180^{\circ}$ and $\beta = 90^{\circ}$, and $\alpha = 90^{\circ}$ and $\beta = 180^{\circ}$, respectively. These local maxima are connected by other local minima. For example, the local minimum at $\alpha = 0^{\circ}$ and $\beta = 180^{\circ}$ is connected with another local minimum at $\alpha = 180^{\circ}$ and $\beta = 180^{\circ}$ via the maximum at $\alpha = 90^{\circ}$ and $\beta = 180^{\circ}$. The energies of local minima at $\alpha = 0^{\circ}$ and $\beta = 180^{\circ}$ and $\alpha = 180^{\circ}$ and $\beta = 0^{\circ}$ are ~21 meV and are easily accessible at room temperature. However, the energy of local minima at $\alpha = 180^{\circ}$ and $\beta = 180^{\circ}$ is ~2 kT at room temperature. These results show that the BCNDTS molecule favors more planar conformation compared to CPs as found in our previous study [20].

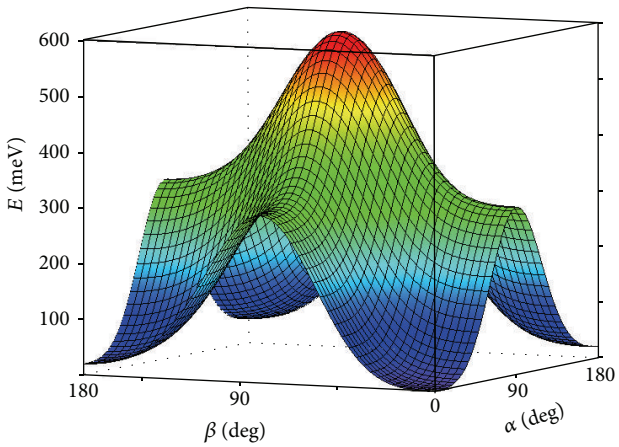

Figure 2: Two-dimensional potential energy surface of the BCNDTS molecule as a function of the two angles α and β.

The form of the potential energy surface (Figure 2) can be understood in terms of the competitions among various interactions such as pi-conjugation, nonbonded repulsive interaction, and hydrogen bonding. The molecular conformation at $\alpha = 0^{\circ}$ and $\beta = 0^{\circ}$ is stabilized by maximum effective pi-conjugation across the backbone chain and by hydrogen bonding between hydrogen and nitrogen atoms. The conformational energy at $\alpha = 180^{\circ}$ and $\beta = 180^{\circ}$ is ~2 kT higher than the one at $\alpha = 0^{\circ}$ and $\beta = 0^{\circ}$ because of the absence of hydrogen bonding and the nonbonded repulsion between nitrogen and sulfur atoms. The maximum of the potential energy surface at $\alpha = 90^{\circ}$ and $\beta = 90^{\circ}$ is accounted for the breakage of pi-conjugation across the backbone chain.

3.2. MEP Surfaces. BCNDTS molecule is composed of three units. Dithienosilole is the central unit, which is connected to cyano groups through 2,1,3-benzothiadiazole moieties.

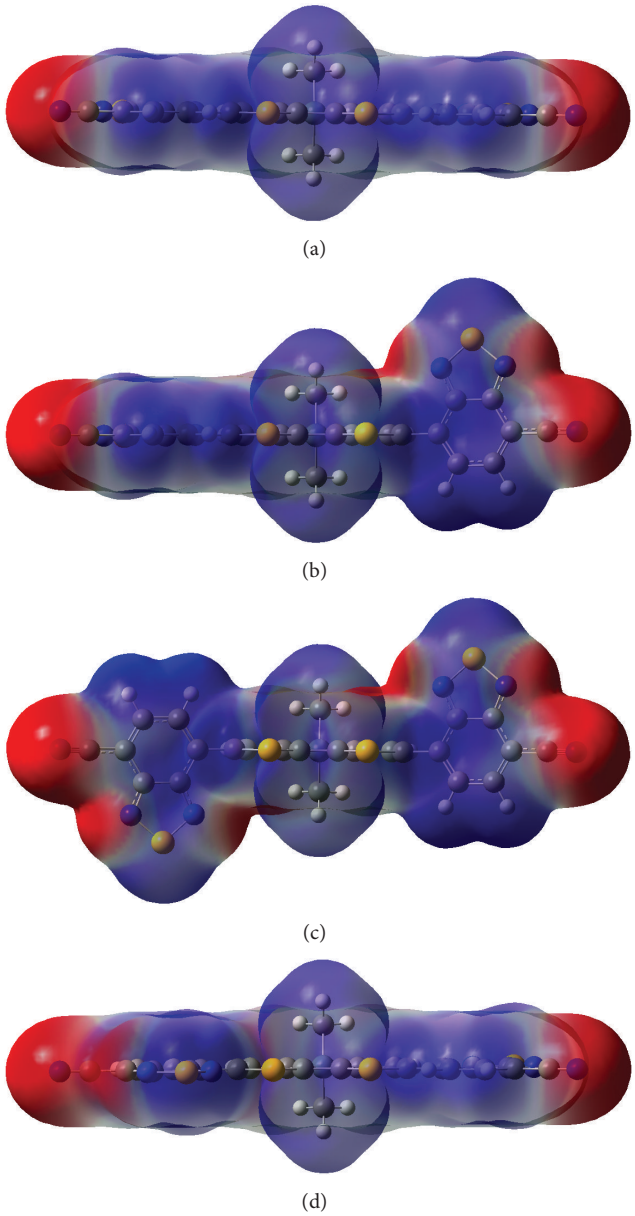

Figure 3: MEP surfaces of the BCNDTS molecule at (a) $\alpha = \beta = 0^{\circ}$, (b) $\alpha = 0$, $\beta = 90^{\circ}$, (c) $\alpha = 90^{\circ}$, $\beta = 90^{\circ}$, and (d) $\alpha = 180^{\circ}$, $\beta = 0^{\circ}$.

Cyano cores are strong electron-withdrawing groups. They pull electron density towards them by exhibiting inductive effect when bonded to 2,1,3-benzothiadiazole units. Consequently, the electron-accepting 2,1,3-benzothiadiazole units also pull electron density from the central dithienosilole unit. As a result, electron densities of cyano units are higher compared to dithienosilole and 2,1,3-benzothiadiazole units. These electron densities can be visualized by constructing three-dimensional molecular electrostatic potential (MEP) surfaces.

Figure 3(a) shows the MEP surfaces of fully relaxed BCNDTS molecule. The region of the MEP surface with blue color represents a lower electron density and has a positive charge. Red color on the MEP surface corresponds

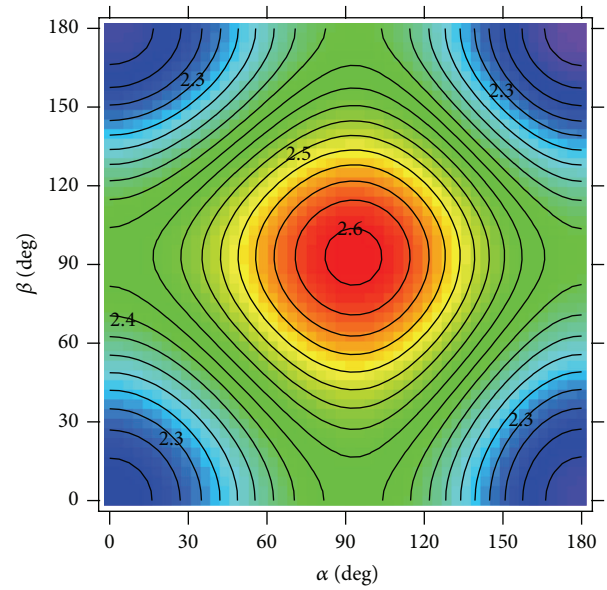

Figure 4: Contour plot of HOMO-LUMO gap of the BCNDTS molecule as a function of the two angles α and β.

to a high electron density and has a negative charge. In the absence of torsional defects, the electron density is uniformly distributed across the BCNDTS molecule with sharp blue color on dithienosilole region and sharp red on cyano region. However, the electron density distribution is affected in the presence of the torsional defect.

At $\alpha = 0^{\circ}$ and $\beta = 90^{\circ}$ (Figure 3(b)), electron density on one 2,1,3-benzothiadiazole region is distinct with more extended red color. Similarly, at $\alpha = 90^{\circ}$ and $\beta = 90^{\circ}$ (Figure 3(c)), the MEP surface of BCNDTS molecule represents the extension of red color on both 2,1,3-benzothiadiazole units compared to the MEP surface without the torsional defect. At $\alpha = 0^{\circ}$ and $\beta = 180^{\circ}$ (Figure 3(d)), MEP surface resembles closely the surface at $\alpha = 0^{\circ}$ and $\beta = 0^{\circ}$. Hence, the extension of red color in the 2,1,3-benzothiadiazole units increases with the breakage of conjugation across the backbone chain.

3.3. HOMO-LUMO Gap. Torsional defect affects not only the energy (Figure 2) and electron density (Figure 3), but also the HOMO-LUMO gap of BCNDTS molecule. As discussed in our previous studies [20, 22] of poly(3-alkylthiophene) and thieno[3,4-b]thiophene-alt-benzodithiophene copolymer, a usual approach for estimating torsional dependence of the HOMO-LUMO gap is to compute the band gap variation when α and β are varied in the range of 0° to 180°. The HOMO-LUMO gap is minimum for planar conformation. It increases with the increase in the torsional angle and reaches the maximum when the two planar-halves are orthogonal to each other.

Figure 4 shows the contour plot of HOMO-LUMO gap for BCNDTS molecule as a function of the two angles, α and β. The two-dimensional HOMO-LUMO gap surface is provided in supporting information (Figure S2). The plot was

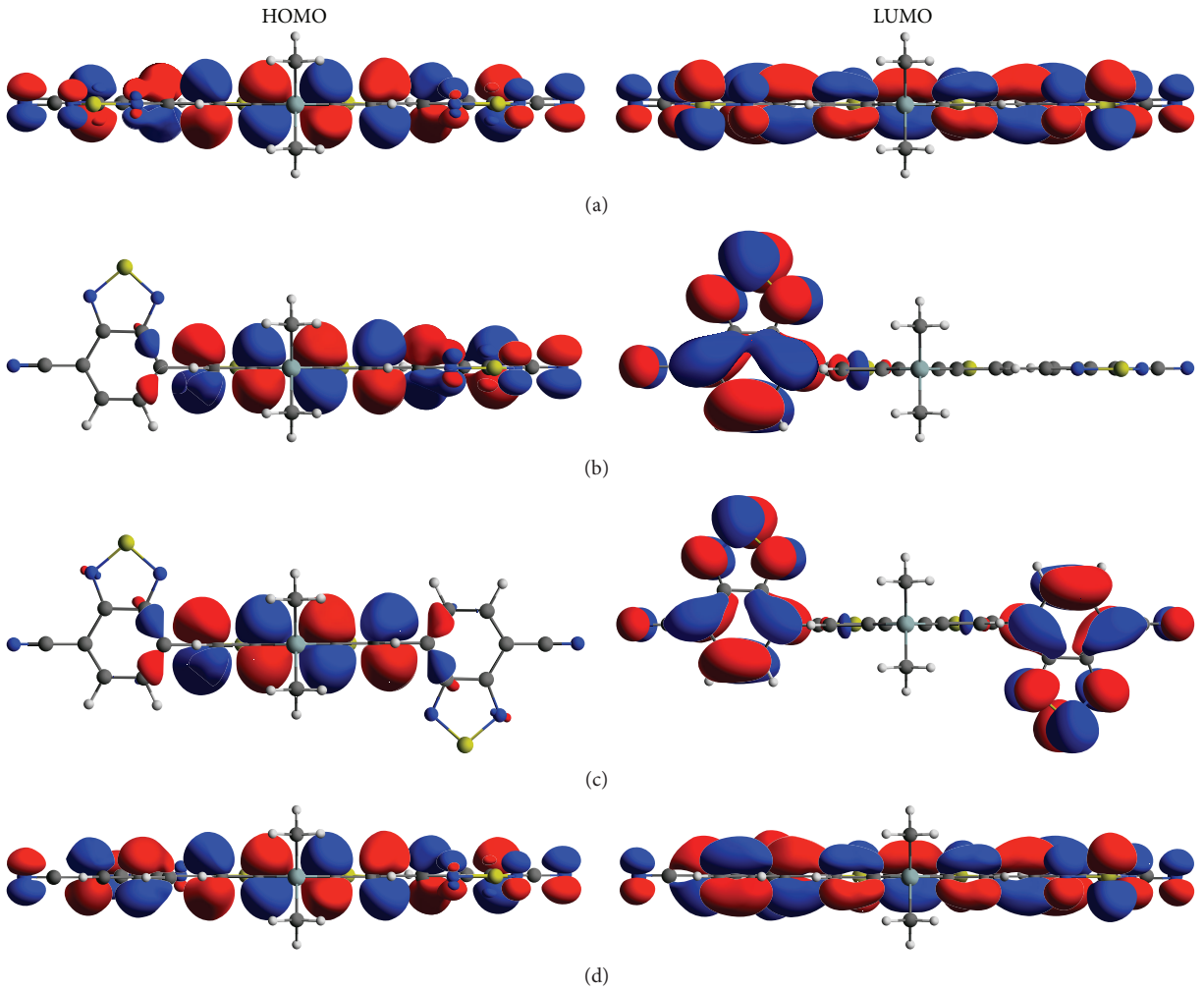

Figure 5: Images of frontier molecular orbitals of the BCNDTS molecule at (a) $\alpha = \beta = 0^{\circ}$, (b) $\alpha = 0$, $\beta = 90^{\circ}$, (c) $\alpha = 90^{\circ}$, $\beta = 90^{\circ}$, and (d) $\alpha = 180^{\circ}$, $\beta = 0^{\circ}$. Red and blue colors represent negative and positive phases of the orbitals, respectively.

generated from the computed forty-nine grid points using the fit function as described in Section 3.1. The root-mean-square residual of the final fit was 0.02 eV. Like the potential energy surface, only one-dimensional terms are significant in the fit of HOMO-LUMO gap.

Figure 4 has a minimum at $\alpha = \beta = 0^{\circ}$ and a maximum at $\alpha = \beta = 90^{\circ}$. The maximum is connected with four local maxima at $\alpha = 0^{\circ}$ and $\beta = 90^{\circ}$, $\alpha = 90^{\circ}$ and $\beta = 0^{\circ}$, $\alpha = 180^{\circ}$ and $\beta = 90^{\circ}$, and $\alpha = 90^{\circ}$ and $\beta = 180^{\circ}$, respectively. The maximum is also connected with four minima at $\alpha = \beta = 0^{\circ}$, $\alpha = 0^{\circ}$ and $\beta = 180^{\circ}$, $\alpha = 180^{\circ}$ and $\beta = 0^{\circ}$, and $\alpha = 180^{\circ}$ and $\beta = 180^{\circ}$, respectively. The HOMO-LUMO gap at $\alpha = 0^{\circ}$ and $\beta = 180^{\circ}$ and at $\alpha = 180^{\circ}$ and $\beta = 180^{\circ}$ are 0.02 eV and 0.04 eV higher, respectively, compared to the HOMO-LUMO gap at $\alpha = 0^{\circ}$ and $\beta = 0^{\circ}$.

The torsional dependence of band gap can be understood in terms of HOMO and LUMO energies. At $\alpha = \beta = 0^{\circ}$ or 180°, the planar geometry favors the effective overlap of p-orbitals resulting in the extended conjugation across the HOMO and LUMO (Figures 5(a) and 5(d)). The overlapping of p-orbitals is decreased as the values of α and β are increased. When α and/or β approach 90°, the extended conjugation is broken as shown in Figures 5(b) and 5(c). Consequently, the energies of HOMO and LUMO get more separated and the band gap of BCNDTS molecule is increased as depicted in Figure 4.

3.4. Excitation Energies. The TDDFT calculations were performed on three representative conformations with $\alpha = 0^{\circ}$ and $\beta = 0^{\circ}$, $\alpha = 0^{\circ}$ and $\beta = 90^{\circ}$, and $\alpha = 90^{\circ}$ and $\beta = 90^{\circ}$ to investigate the effect of torsional defect on excitation energies and the oscillator strength. Figure 6 shows the computed UV/VIS spectra for the representative conformations with their oscillator strengths. The planar conformation ($\alpha = \beta = 0^{\circ}$) has the vertical excitation energy of ~2 eV from the ground (S_0) state to the first excited singlet (S_1) state with the highest oscillator strength of ~1.2. At $\alpha = 0^{\circ}$ and $\beta = 90^{\circ}$, the spectrum is blue shifted by ~ 0.3 eV. At $\alpha = 90^{\circ}$ and $\beta = 90^{\circ}$, the spectrum is further blue shifted with the reduced oscillator strength of ~0.8.

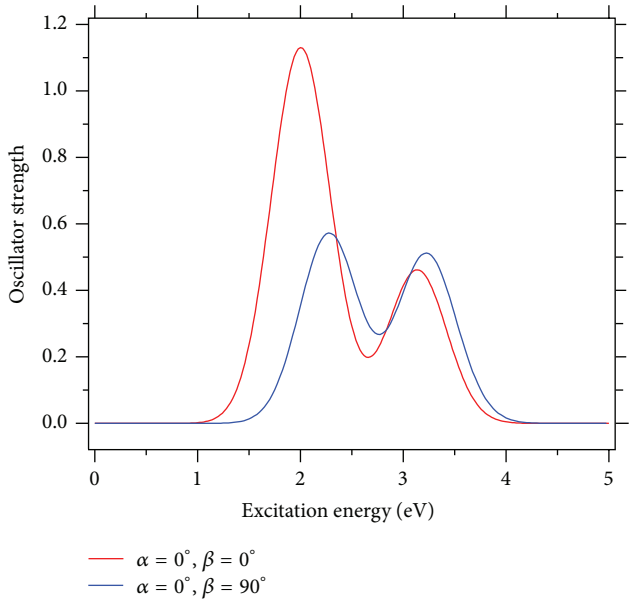

Figure 6: Computed UV/VIS spectra of the BCNDTS molecule at different torsional angles.

The transition from S_0 to S_1 represents the promotion of an electron from HOMO to LUMO. Stronger peak in Figure 6 for the planar conformation represents the electronic transition from HOMO to LUMO and a weaker peak represents the electronic transition from HOMO to LUMO+2 (with the oscillator strength of ~0.3). At $\alpha = 0^\circ$ and $\beta = 90^\circ$, BCNDTS molecule shows two peaks with the oscillator strength of ~0.5. These peaks represent the electronic transition from HOMO to LUMO+1 and HOMO-1 to LUMO+1, respectively. At the maximum torsional defect ($\alpha = \beta = 90^\circ$), BCNDTS molecule shows a peak with the oscillator strength of ~0.7, which represents the transition from HOMO-2 to LUMO or HOMO to LUMO+2. There are two important effects of torsional defects: (i) the oscillator strength decreases with the increase in torsional defects and (ii) the spectrum is blue shifted with the increase in torsional defects. These results indicate that the torsional defects present in BCNDTS molecule decrease the OPV performance, thereby reducing the strength of π-π^* transition.

4. Conclusions

DFT and TDDFT calculations were performed to investigate the structural and electronic properties of BCNDTS molecule. Two-dimensional potential energy surface as function of interring torsional angles and energies of frontier molecular orbitals were computed using dispersion corrected B3LYP functional. The ground state electronic properties calculated at the dispersion corrected B3LYP were found to be in good agreement with the available experimental values. The vertical excitation energies were calculated starting from the ground state optimized geometries at the dispersion corrected B3LYP level.

In the present investigation, the lowest energy structure of BCNDTS molecule was found to have planar conformation. The planar conformation was found to favor the lowest HOMO-LUMO gap and excitation energies but the highest oscillator strength. The oscillator strength was found to be decreased and the absorption spectrum was found to be blue shifted for higher energy conformations caused by the torsional defects. The present study suggests that small conjugated molecules containing central dithienosilole cores connected with 2,1,3-benzothiadiazole groups, which favor the lowest energy planar conformation, have potential to be an efficient electron donor for OPV devices.

Conflict of Interests

The authors declare that there is no conflict of interests regarding the publication of this paper.

Acknowledgments

The authors are grateful to the National Science Foundation (Grant no. DMR0847580) for financial support. This work used the Extreme Science and Engineering Discovery Environment (XSEDE), which is supported by National Science Foundation Grant no. ACI-1053575. The authors thank additional support from the University of Akron.

References

[1] C. J. Brabec, N. S. Sariciftci, and J. C. Hummelen, "Plastic solar cells," *Advanced Functional Materials*, vol. 11, no. 1, pp. 15–26, 2001.

[2] H. Hoppe and N. S. Sariciftci, "Organic solar cells: an overview," *Journal of Materials Research*, vol. 19, no. 7, pp. 1924–1945, 2004.

[3] N. Serdar Sariciftci, "Plastic photovoltaic devices," *Materials Today*, vol. 7, no. 8, pp. 36–40, 2004.

[4] S. B. Darling and F. You, "The case for organic photovoltaics," *RSC Advances*, vol. 3, no. 39, pp. 17633–17648, 2013.

[5] Z. He, C. Zhong, S. Su, M. Xu, H. Wu, and Y. Cao, "Enhanced power-conversion efficiency in polymer solar cells using an inverted device structure," *Nature Photonics*, vol. 6, no. 9, pp. 591–595, 2012.

[6] J. Roncali, P. Leriche, and P. Blanchard, "Molecular materials for organic photovoltaics: small is beautiful," *Advanced Materials*, vol. 26, no. 23, pp. 3821–3838, 2014.

[7] J. Roncali, P. Frère, P. Blanchard et al., "Molecular and supramolecular engineering of π-conjugated systems for photovoltaic conversion," *Thin Solid Films*, vol. 511-512, pp. 567–575, 2006.

[8] Y. Sun, G. C. Welch, W. L. Leong, C. J. Takacs, G. C. Bazan, and A. J. Heeger, "Solution-processed small-molecule solar cells with 6.7% efficiency," *Nature Materials*, vol. 11, no. 1, pp. 44–48, 2012.

[9] L.-Y. Lin, C.-W. Lu, W.-C. Huang, Y.-H. Chen, H.-W. Lin, and K.-T. Wong, "New A-A-D-A-A-type electron donors for small molecule organic solar cells," *Organic Letters*, vol. 13, no. 18, pp. 4962–4965, 2011.

[10] S. Roquet, A. Cravino, P. Leriche, O. Alévêque, P. Frère, and J. Roncali, "Triphenylamine-thienylenevinylene hybrid systems

with internal charge transfer as donor materials for heterojunction solar cells," *Journal of the American Chemical Society*, vol. 128, no. 10, pp. 3459–3466, 2006.

[11] J. Zhou, X. Wan, Y. Liu et al., "Small molecules based on benzo[1,2-b:4,5-b′]dithiophene unit for high-performance solution-processed organic solar cells," *Journal of the American Chemical Society*, vol. 134, no. 39, pp. 16345–16351, 2012.

[12] H. Lu, C. Lu, Y. Lee et al., "New molecular donors with dithienopyrrole as the electron-donating group for efficient small-molecule organic solar cells," *Chemistry of Materials*, vol. 26, no. 15, pp. 4361–4367, 2014.

[13] H.-C. Ting, Y.-H. Chen, L.-Y. Lin et al., "Benzochalcogenodiazole-based donor-acceptor-acceptor molecular donors for organic solar cells," *ChemSusChem*, vol. 7, no. 2, pp. 457–465, 2014.

[14] D. Demeter, S. Mohamed, A. Diac, I. Grosu, and J. Roncali, "Small molecular donors for organic solar cells obtained by simple and clean synthesis," *ChemSusChem*, vol. 7, no. 4, pp. 1046–1050, 2014.

[15] A. Mishra and P. Bäuerle, "Small molecule organic semiconductors on the move: promises for future solar energy technology," *Angewandte Chemie - International Edition*, vol. 51, no. 9, pp. 2020–2067, 2012.

[16] P. Hohenberg and W. Kohn, "Inhomogeneous electron gas," *Physical Review*, vol. 136, pp. B864–B871, 1964.

[17] A. D. Becke, "Density-functional thermochemistry. III. The role of exact exchange," *The Journal of Chemical Physics*, vol. 98, no. 7, pp. 5648–5652, 1993.

[18] M. J. Frisch, G. W. Trucks, H. B. Schlegel et al., *Gaussian 09, Revision D.01*, Gaussian Inc., Wallingford, Conn, USA, 2009.

[19] S. Grimme, "Semiempirical GGA-type density functional constructed with a long-range dispersion correction," *Journal of Computational Chemistry*, vol. 27, no. 15, pp. 1787–1799, 2006.

[20] R. S. Bhatta, D. S. Perry, and M. Tsige, "Nanostructures and electronic properties of a high-efficiency electron-donating polymer," *The Journal of Physical Chemistry A*, vol. 117, no. 47, pp. 12628–12634, 2013.

[21] R. S. Bhatta and D. S. Perry, "Correlated backbone torsional potentials in poly(3-methylthiophene)," *Computational and Theoretical Chemistry*, vol. 1008, pp. 90–95, 2013.

[22] R. S. Bhatta, M. Tsige, and D. S. Perry, "Torsionally-induced blue shift of the band gap in poly(3-hexylthiophene)," *Journal of Computational and Theoretical Nanoscience*, vol. 11, no. 10, pp. 2157–2164, 2014.

[23] M. D'Auria, L. Emanuele, and R. Racioppi, "Regio- and stereoselectivity in the Paternò-Büchi reaction on furan derivatives," *International Journal of Photoenergy*, vol. 2006, Article ID 84645, 11 pages, 2006.

[24] T. Chokbunpiam, P. Thamyongkit, O. Saengsawang, and S. Hannongbua, "Molecular structure and electronic properties of porphyrin-thiophene-perylene using quantum chemical calculation," *International Journal of Photoenergy*, vol. 2010, Article ID 492313, 8 pages, 2010.

[25] T. Yakhanthip, N. Kungwan, J. Jitonnom, P. Anuragudom, S. Jungsuttiwong, and S. Hannongbua, "Theoretical investigation on the electronic and optical properties of poly(fluorenevinylene) derivatives as light-emitting materials," *International Journal of Photoenergy*, vol. 2011, Article ID 570103, 9 pages, 2011.

[26] E. Runge and E. K. U. Gross, "Density-functional theory for time-dependent systems," *Physical Review Letters*, vol. 52, no. 12, pp. 997–1000, 1984.

[27] T. Yanai, D. P. Tew, and N. C. Handy, "A new hybrid exchange-correlation functional using the Coulomb-attenuating method (CAM-B3LYP)," *Chemical Physics Letters*, vol. 393, no. 1–3, pp. 51–57, 2004.

[28] H. Iikura, T. Tsuneda, T. Yanai, and K. Hirao, "A long-range correction scheme for generalized-gradient-approximation exchange functionals," *Journal of Chemical Physics*, vol. 115, no. 8, pp. 3540–3544, 2001.

[29] J.-D. Chai and M. Head-Gordon, "Long-range corrected hybrid density functionals with damped atom-atom dispersion corrections," *Physical Chemistry Chemical Physics*, vol. 10, no. 44, pp. 6615–6620, 2008.